HYPERELASTIC CONSTITUTIVE MODELS FOR INCOMPRESSIBLE ELASTOMERS AND SOFT TISSUES: FITTING AND PERFORMANCE COMPARISON

Leonardo Hoss, hoss.lhoss@yahoo.com.br
Rogério José Marczak, rato@mecanica.ufrgs.br
Departamento de Engenharia Mecânica – UFRGS
Rua Sarmento Leite, 425 – Porto Alegre – RS – Brasil - 90050170

Abstract. *The present work presents a study on several constitutive models for incompressible elastomers and soft tissues published in the technical literature. Classical models are considered as well as recent contributions to the field. The corresponding expressions for the strain energy are implemented in a computational code to recover the constitutive constants for each model through the optimization of the differences between theoretical and experimental stress (calibration), the later obtained from uniaxial tensile, pure shear and biaxial tensile testings. The theoretical stress predictions are compared against experimental values for two samples of elastomers under different strain ranges, allowing a subjective analysis comparing all models, and a discussion about the performance of each one. An estimator is proposed to evaluate quantitatively the goodness of fit of the theoretical predictions with the experimental curves, as a substitute for correlation coefficients which are not suited to non-linear curve fitting. The proposed estimator is tested for the samples under several strain ranges, and it is shown its efficiency as an aid to select the best models for a given application. Many of the models studied here cannot deliver satisfactory theoretical predictions for deformation modes different from the used in the calibration. Therefore, a compromise optimization scheme is investigated in order to improve the quality of faulty predictions without destroying the good ones.*

Keywords*: Hyperelastic constitutive models, Goodness of fit, Compromise optimization*

1. INTRODUCTION

The evolution of the constitutive models for hyperelastic materials and soft tissues is strongly marked by a proliferation of models during the last decade. These hyperelastic models can be grouped hierarchically according with their genealogy and chronology in five general families, as illustrated in Fig. 1.

A common issue in the selection and validation of hyperelastic models is the absence of ranking criteria which, along with the large variety of models available, makes the selection process difficult, subjective, and highly susceptible of misinterpretation task. The usual ways for measuring the quality of the fit is through the evaluation of relative errors between the theoretical predictions and the experimental curves, or alternatively, directly by visual inspection of the plots. Any of these methodologies are inefficient when one is looking for an accurate analysis of each model as, for example, when understanding the influence of a specific term of the strain energy density function. A more significant and useful parameter is the regression coefficient, which contains minimal information about the fitting: the near the unity, the better is the fit. Regression coefficients are, however, unsuitable for nonlinear regressions like the ones found in calibration of elastomers. This concept will be the base for developing a specific goodness of the fit estimator in the present work.

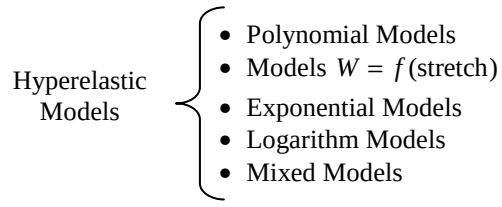

Figure 1. Common types of hyperelastic models.

2. CLASSICAL AND NON-CLASSICAL HYPERELASTIC MODELS

Modern design practices in rubber industry are largely based on finite element simulations, and the accuracy of these relies on the ability of the constitutive model used in predicting the mechanical behavior of the material. Therefore, the main point when modeling a particular hyperelastic material is the selection of a suitable constitutive equation. The present work considers several constitutive models available in the literature for incompressible materials. Most constitutive models can be roughly grouped in one of two broad categories: phenomenological and micromechanical models, as illustrated in Fig. 2. Details about the strain energy functions studied here can be found in Hoss (2009).

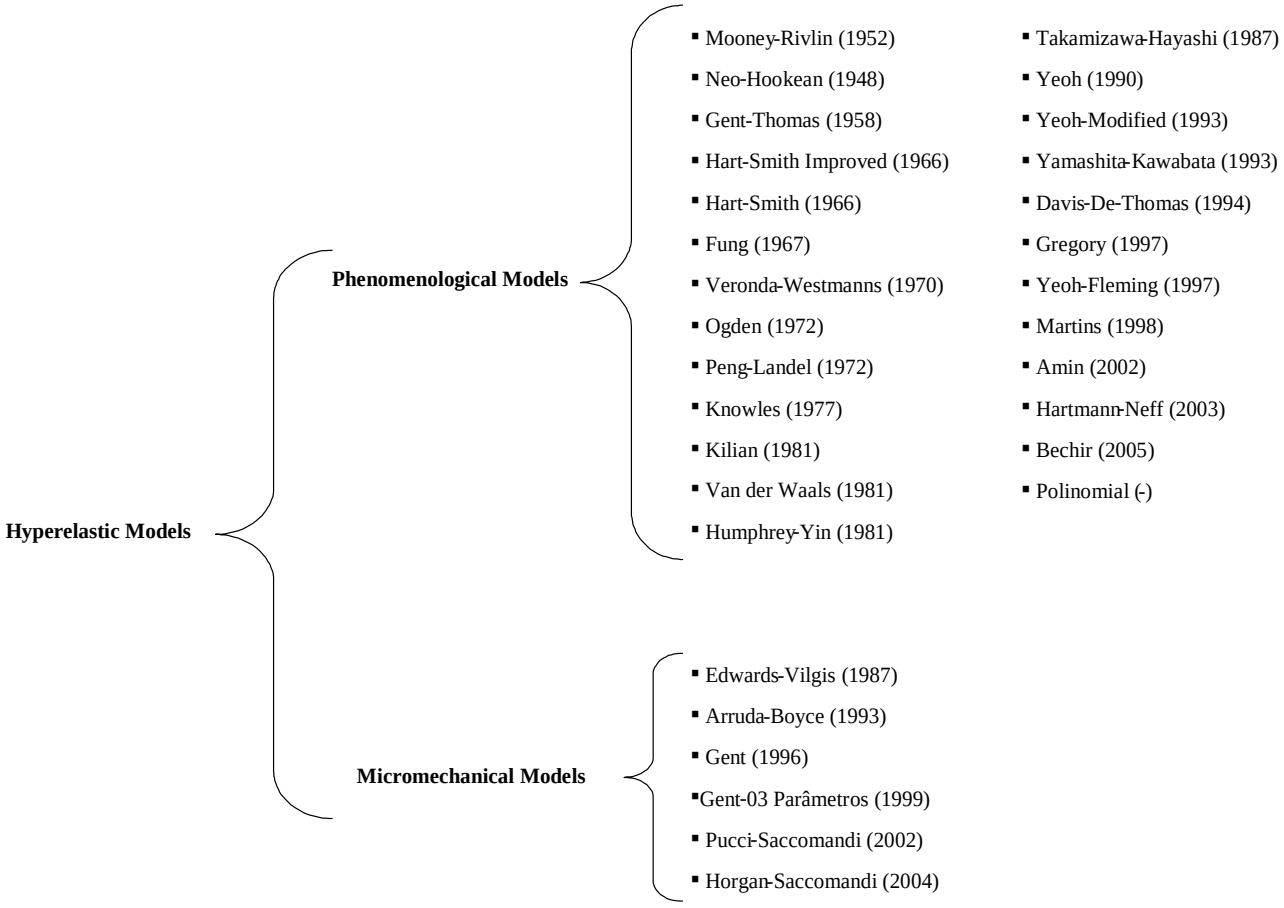

Figure 2. Classification of several hyperelastic models reported in the literature.

After a deep examination of the historical and mathematical details of the models shown in Fig. 2, ten hyperelastic families can be suggested as listed in Tab. 1. This proposal is a tentative sub-classification which aims to group the several models according to their similarities in the analytic formulation, relationship with other models, or by chronological proximity of the original publications. This classification – one of the contributions of the present work – is suggested not only to reduce the amount of results plots, but also to group those models with behavior and features potentially (but not necessarily) similar. Therefore, it is expected that the advantages and disadvantages, as well as fitting and prediction patterns are shared among the members of each group, although this rule has been violated in many cases (for example, when the association is purely chronological).

In practice, it is impossible to make definitive statements about the usage for of each model, but after an extensive set of tests using different materials, very general rules of application for each model can be traced. Figure 3 presents a gross suggestion of deformation limits to employ the models reviewed in Fig.2 (Hoss, 2009).

3. CURVE FITTING

The present work employs two samples of material: Treloar's data (Treloar, 1975) and natural rubber NR55 (Marczak, *et al.*, 2006). Figure 4 shows a visual graphical analysis of the models MRI9 and PSI fitted for Treloar's data in uniaxial test up to a maximum deformation (e) of 700%. The convention used for the stress vs. strain curve $(t \times e)$ in this and all other figures is as follows: experimental results are plotted with dashed lines, while theoretical predictions are continuous lines. Uniaxial tensile (T) tests are plotted in black, with pure-shear (S) tests in blue and biaxial (B) tensile tests in red. As mentioned by Humphrey (2002, 2003), if the characteristic stiffening of the elastomer is significant and starts to occur at moderate strains, many classical hyperelastic models (like Mooney-Rivlin, Blatz-Ko and others) cannot deliver good results. Although a particular model may fit the experimental results very well, the same may not happen with the theoretical predictions for other loadings, a fact commonly omitted in many cases in the literature. Results for the MRI9 model shown in Fig.4 illustrate one of such cases, while the PSI model exemplifies the opposite case, delivering good predictions for deformation modes different from the one used in the calibrations of the constitutive constants.

Table 1. Hyperelastic groups.

HYPERELASTIC GROUPS					
GROUP$_1$	**MRI2**	*Mooney Rivlin (N=2)*	**GROUP$_6$**	**PLI**	*Peng e Landel*
	MRI3	*Mooney Rivlin (N=3)*		**MI**	*Martins*
	MRI5	*Mooney Rivlin (N=5)*		**KLI**	*Kilian*
	MRI9	*Mooney Rivlin (N=9)*		**VDWI**	*Van der Waals*
GROUP$_2$	**HNI1**	*Hartmann e Neff (N=1)*	**GROUP$_7$**	**YI2**	*Yeoh (N=2)*
	HNI2	*Hartmann e Neff (N=9)*		**YI3**	*Yeoh (N=3)*
	HNI3	*Hartmann e Neff (N=9)*		**YI5**	*Yeoh (N=5)*
	PI3	*Polynomial (N=9)*		**YMI**	*Yeoh Modified*
GROUP$_3$	**NHI**	*Neo-Hookean*	**GROUP$_8$**	**YKI**	*Yamashita-Kawabata*
	GTI	*Gent-Thomas*		**AI**	*Amin*
	HSAI	*Hart-Smith Improved*		**DTI**	*Davis-De-Thomas*
	HSI	*Hart-Smith*		**GYI**	*Gregory*
GROUP$_4$	**FI**	*Fung*	**GROUP$_9$**	**THI**	*Takamizawa-Hayashi*
	VWI	*Veronda-Westmanns*		**EVI**	*Edwards-Vilgis*
	KI	*Knowles*		**ABI5**	*Arruda-Boyce*
	HYI	*Humphrey-Yin*		**GI**	*Gent*
GROUP$_5$	**OI2**	*Ogden (N=2)*	**GROUP$_{10}$**	**YFI**	*Yeoh-Fleming*
	OI3	*Ogden (N=3)*		**G3I**	*Gent a 03 Parameters*
	HBI2	*Bechir (N=2)*		**PGSI**	*Pucci-Saccomandi*
	HBI3	*Bechir (N=3)*		**HGSI**	*Horgan- Saccomandi*

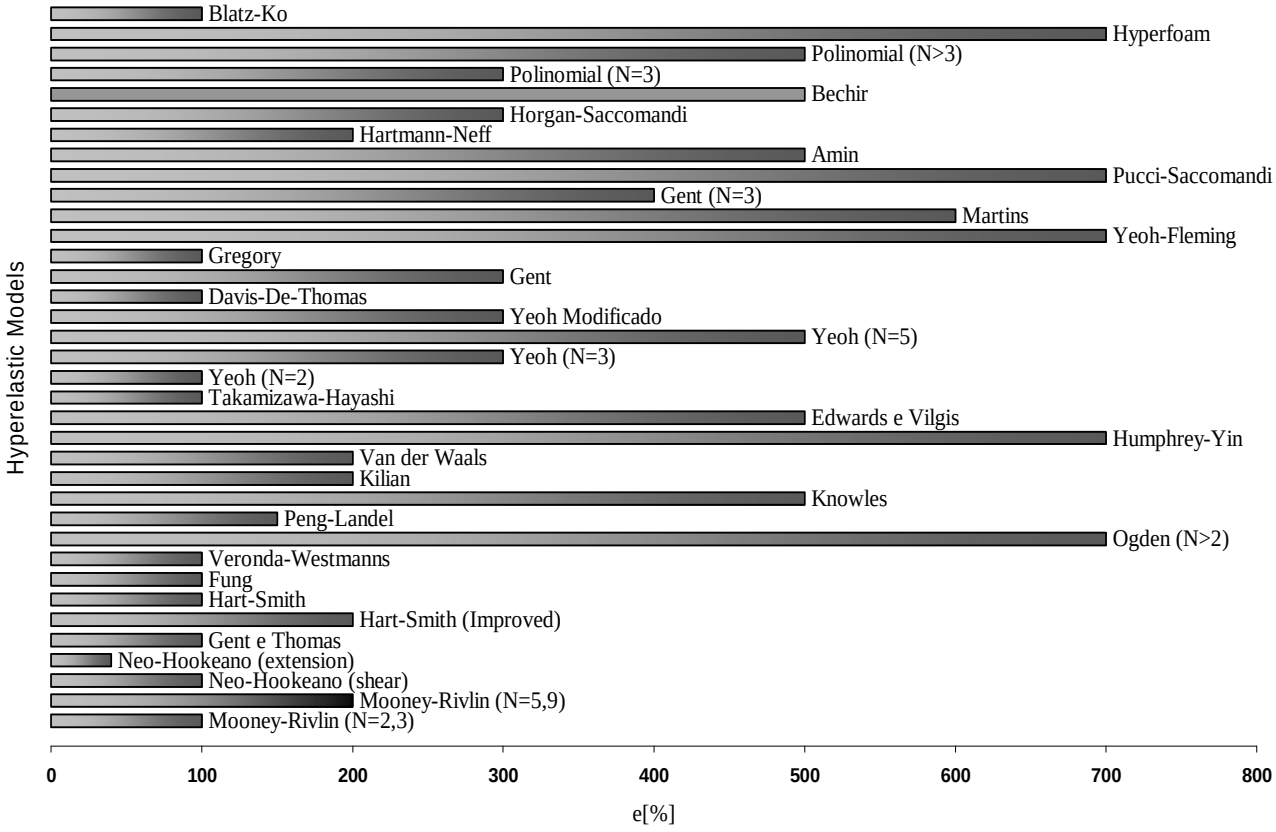

Figure 3. Gross limits of application for hyperelastic models.

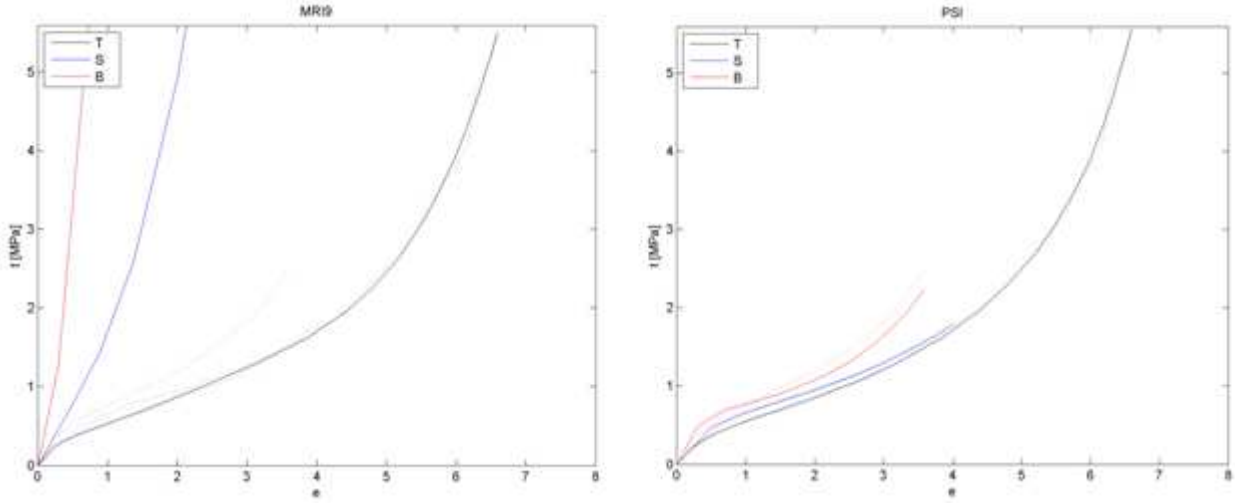

Figure 4. Curve fitting and prediction results for MRI9 and PSI models.

As shown in the example of Fig. 4, a purely visual assessment of a given constitutive model may be very misleading, making the selection process susceptible to errors and misinterpretation. A method used by many authors for check the quality of the fit and the predictions is to calculate the relative errors between theoretical and experimental results. This percentage error is given:

$$\text{Residual Error (\%)} = \frac{\left|t_e(\lambda) - t_t(\lambda)\right|}{t_e(\lambda)} \times 100 \tag{1}$$

where $t_e(\lambda)$ e $t_t(\lambda)$ corresponds to the experimental and numerical stress values, respectively.

Figure 5 shows an analysis using this concept for two constitutive models, and it exemplifies an actual situation where the analyst cannot be confident about choosing one of them using Eq. (1). Both models were fitted to uniaxial tension $(0 \le e \le 700\%)$ using the Treloar's data and, despite the good performance of the Gent's model (GI), Eq. (1) seems to indicate the contrary. This is a bad characteristic of Eq. (1), since it does not take into account the relative magnitude of the stresses involved along the deformation range.

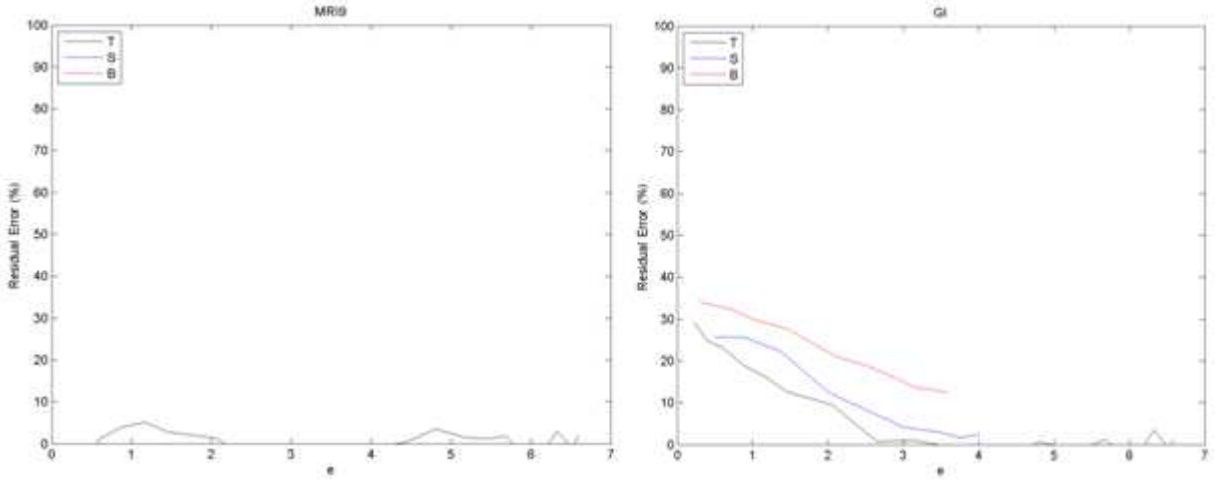

Figure 5. Residual error between experimental and theoretical results measured by Eq. (1).

4. A NEW ERROR ESTIMATOR PROPOSAL

The derivation of a more suitable error estimator to verify and compare the quality of the fittings should obey three basic rules. First, it has to be compatible with non-linear regressions, since this is the case when dealing with hyperelastic constitutive models. This is not the case of the linear regression (r^2) commonly used in the literature.

Second, the estimator must be of simple computational implementation. Such estimator could be therefore included in commercial software to help the analyst to choose among so many models available in them, something currently left to the user. And at last, the estimator must be mathematically consistent in order to reflect faithfully the behavior and quality of the fitting and theoretical predictions, regardless the deformation/stress range. Using these rules, the following estimator is proposed, based on the same concept of the linear regression coefficient, but adapted for non-linear curve fitting:

$$r^2 = 1 - \frac{S_{reg}}{S_{Stot}}$$
$$S_{reg} = \sum_{i=1}^{n} \left(t_e - t_t\right)^2 \tag{2}$$
$$S_{Stot} = \sum_{i=1}^{n} w_i \left(t_e - \overline{t_e}\right)^2$$

where t_e and t_t are the experimental and theoretical stress values, respectively. In general, the r^2 coefficient is computed from de sum of the squares of the differences using from the best curve obtained by a non-linear regression. This sum of the squares is called S_{reg}, which has the same units of the variables in the vertical axis, but squared. In order to normalize the estimator, S_{reg} is divided by the sum of the squares of the difference to the mean value up to the point in question, S_{Stot}. If the curve fits the data satisfactorily, S_{reg} will be much smaller than S_{Stot}. Figure 6 illustrates these ideas.

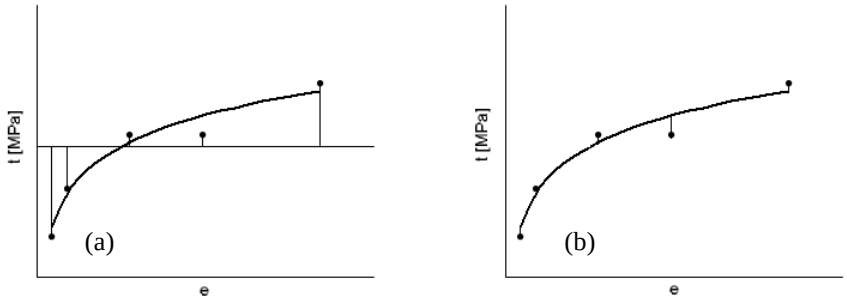

Figure 6. Evaluation of the new estimator. (a) Interpretation of S_{Stot}. (b) Interpretation of S_{reg}.

In to provide an assessment of Eq. (2), it was tested the most representative models of each hyperelastic family of Tab.1. In the next examples, it is shown that Eq. (2) can be effectively used not only as an indicator to aid the selection of hyperelastic models, but also as a comparison parameter between two or more models. In order to avoid proliferation of graphs, the results will be presented only for uniaxial and biaxial tests. The estimator are presented by bar diagrams representing the lowest value obtained in the deformation range, for the deformation mode used in the calibration and the other deformation modes as well. This provides an indication of the goodness of fit for deformation modes other than the one used in the calibration.

4.1 Natural Rubber – Large Deformations

Treloar's data (Treloar, 1975) were used to calibrate the constants in the following deformation ranges: $0 \le e \le 700\%$ for uniaxial stress, $0 \le e \le 400\%$ for pure shear, and $0 \le e \le 350\%$ for biaxial stress.

4.1.1 Fitting for uniaxial tensile test

The hyperelastic constants were obtained with the experimental data in the range $0 \le e \le 700\%$. At the end of each deformation increment of 100% a new set of constants was fitted, and Eq. (2) was evaluated for the uniaxial mode as well as for the predictions (pure shear and biaxial stress). The lowest values obtained for each increment is plotted in Fig. 7 for the models MRI9, OI2, KI, YI3, GI and PSI.

Note that through plots such as Fig. 7 an engineering analyst, even without a deep knowledge in hyperelasticity, can easily conclude that the PSI model is the best in this particular case. The good overall performance of the PSI model can be confirmed by the plots in Fig. 8, showing the theoretical predictions superimposed to the experimental data, and the behavior of the Eq. (2) along the deformation range.

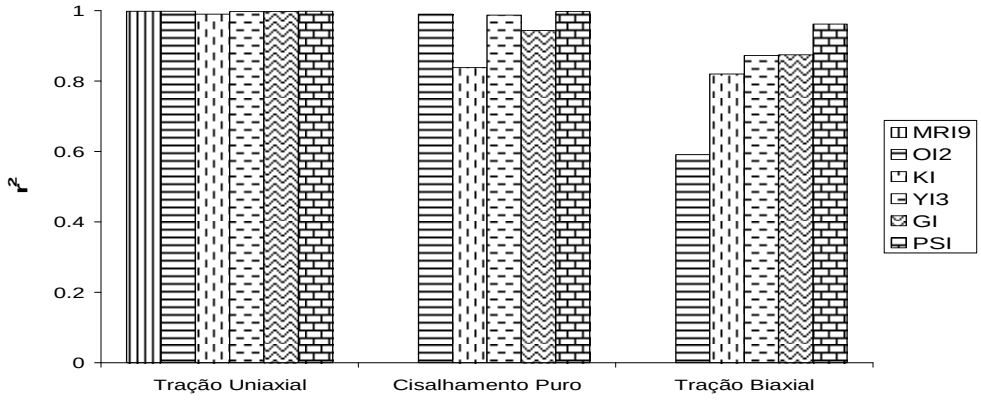

Figure 7. Performance comparison of some hyperelastic models using Eq. (2) – calibration for uniaxial stress.

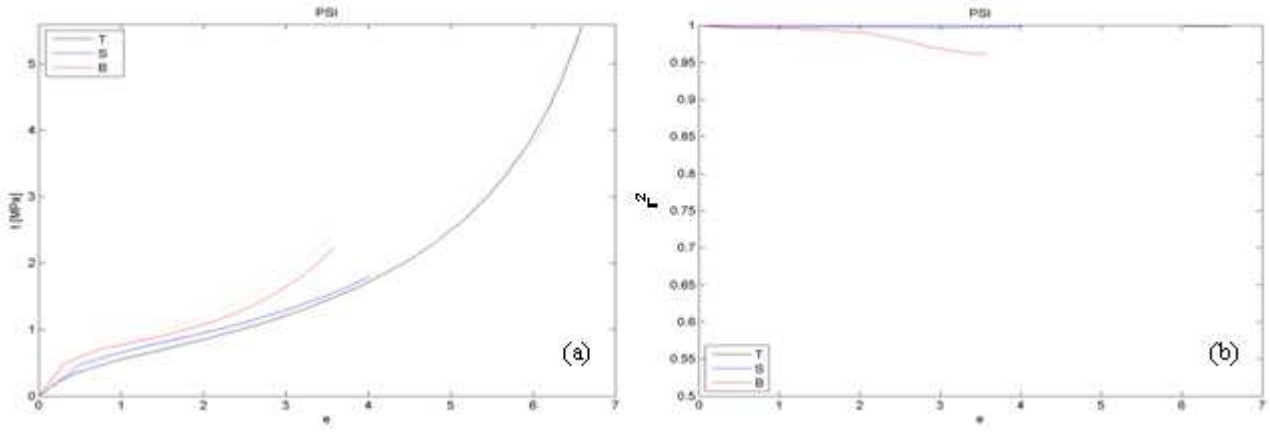

Figure 8. Performance of the PSI model. (a) Curve fitting. (b) Error estimator by Eq. (2).

4.1.2 Fitting for biaxial tensile test

In this case the constants were obtained with the experimental data in the range $0 \le e \le 350\%$. The same procedure used in section 4.1.1 was used. The estimator plotted in Fig.9 suggests that the calibration using biaxial stress may not be better than using uniaxial stress, as openly reported in the literature. Again the PSI model presented better performance than the other models.

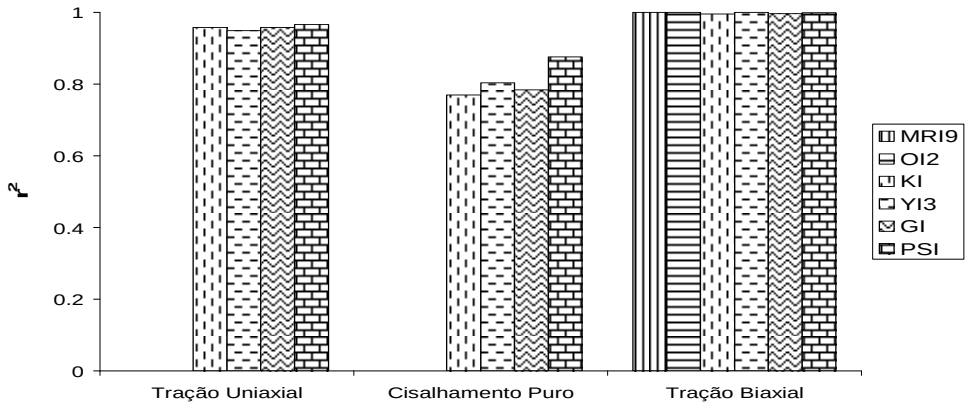

Figure 9. Performance comparison of some hyperelastic models using Eq. (2) – calibration for biaxial stress.

4.2 Natural Rubber – Small Deformations

In order to assess the behavior of the hyperelastic models in deformation ranges significantly narrower than the ones studied in section 4.1, here another sample of natural rubber will be used - NR55 (Marczak, *et al*., 2006). The deformation ranges used for each test are: $0 \le e \le 100\%$ for uniaxial stress, $0 \le e \le 130\%$ for pure shear, and $0 \le e \le 70\%$ for biaxial stress.

4.2.1 Fitting for uniaxial tensile test

The hyperelastic constants were obtained for the experimental data in the range $0 \le e \le 100\%$. At the end of each deformation increment of 10% a new set of constants was fitted, and Eq. (2) was evaluated for the uniaxial mode as well as for the predictions (pure shear and biaxial stress).

Figure 10 compares the estimator obtained for the models MRI9, OI2, KI, YI3, GI and PSI. In this case the YFI model presented the best overall performance. It is worth to note that some models (MRI9 and PSI) generated useless predictions, in spite of the good fit for the uniaxial stress. In order to prove this, Fig. 11 presents the theoretical predictions and the behavior of the Eq. (2) along the deformation range for the PSI model, in perfect agreement to Fig.10.

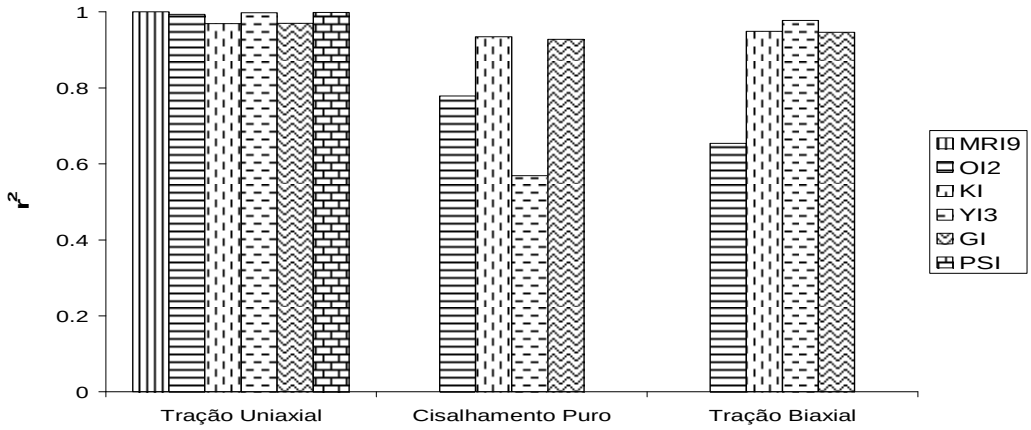

Figure 10. Performance comparison of some hyperelastic models using Eq. (2) – calibration for uniaxial stress.

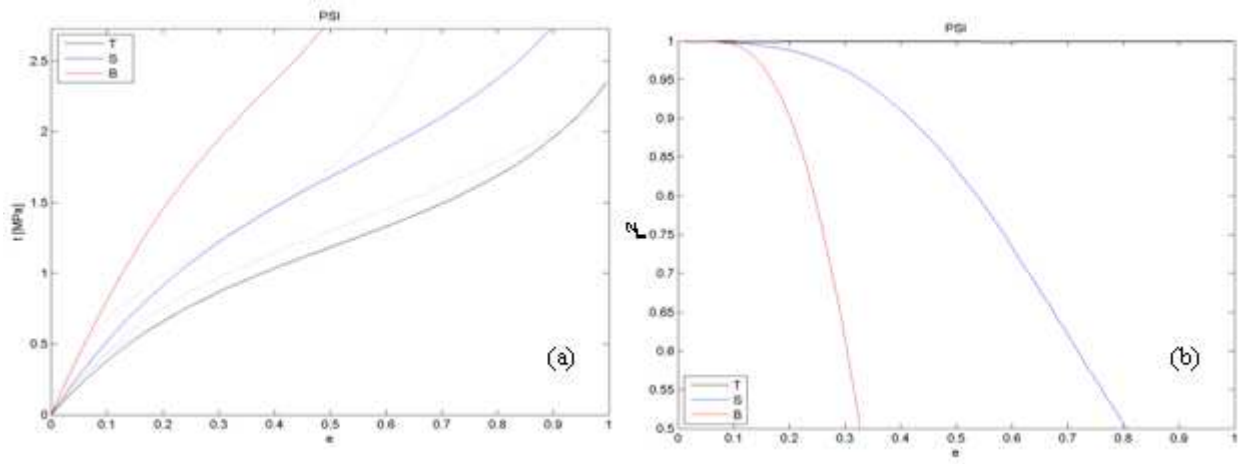

Figure 11. Assessment of PSI model. (a) Graphics analysis. (b) Analysis using the Eq. (2).

4.2.2 Fitting for biaxial tensile test

The hyperelastic constants were obtained with the experimental data in the range $0 \le e \le 70\%$ and, again, at the end of each deformation increment of 10% a new set of constants was fitted, and Eq. (2) was evaluated for the biaxial mode as well as for the predictions (pure shear and uniaxial stress). Figure 12 compares the performance of the models MRI9, OI2, KI, YI3, GI, and PSI. Clearly the YFI model performs better than the others.

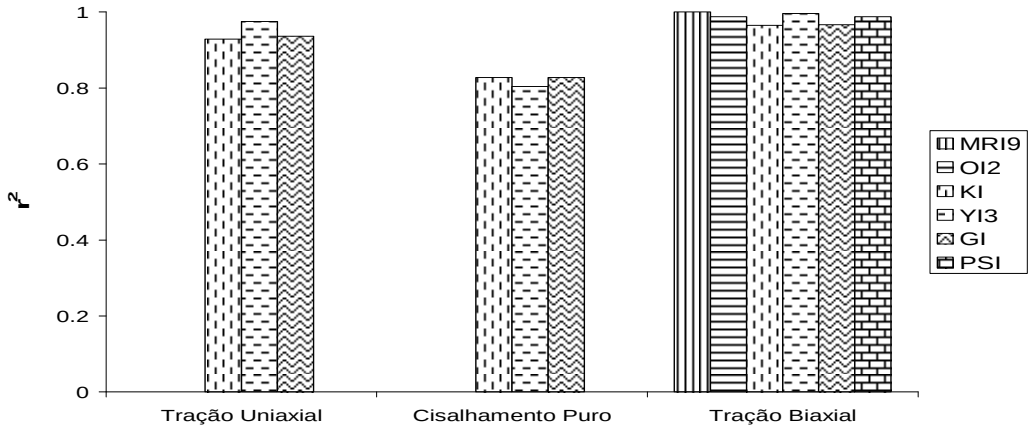

Figure 12. Performance comparison of some hyperelastic models using Eq. (2) – calibration for biaxial stress.

5. COMPROMISE OPTIMIZATION

Ideally, the best way to calibrate the constants for general applications would be to optimize them in a single pass using a multi- criteria cost function. However, the total stretches of each deformation mode are generally very different. An optimization considering the smallest deformation range of all three testing (biaxial testing) would neglect a significant part of the uniaxial and shear experimental data. A possible solution is to employ a compromise optimization, based on a linear combination of the constants calibrated for each deformation mode:

$$\overline{C} = w_T C_T + w_P C_P + w_B C_B \tag{3}$$

where $\overline{C}$ is a new set of average constitutive constants, w_T, w_P, w_B represent the weights for the groups of constants of the uniaxial tensile (C_T), pure shear (C_P) and biaxial tensile (C_B) testing, respectively. Equation (3) does not represent a global optimum, but on the other hand it allows one to tune the importance of each mode by changing the corresponding weight suitably. The following cases are studied in the present work: Case 1, same weights for all tests $(w_T = w_P = w_B = 1/3)$; Case 2, majoring the importance of the biaxial mode $(w_T = w_P = 1/4, w_B = 1/2)$; and Case 3, majoring the importance of the uniaxial mode $(w_T = 1/2, w_P = w_B = 1/4)$. All cases used Treloar's data.

Figure 13 showing that the compromise optimization for the YI3 model not only improved the predictions of the biaxial test, but also generated acceptable curves for the three tests.

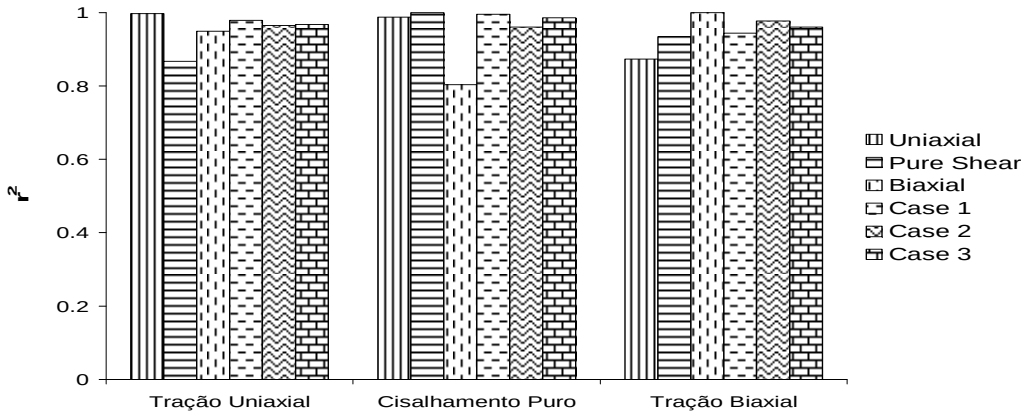

Figure 13. Compromise optimization results for YI3 model.

Figure 14 compares the predictions obtained for the YI3 model using the constants calibrated for the uniaxial testing (Fig. 14a) with the predictions obtained for Case 1 (Fig. 14b). It is clear that the improvement obtained for the biaxial mode using Eq. (3) did not imply in a visible degradation of the predictions for the other modes.

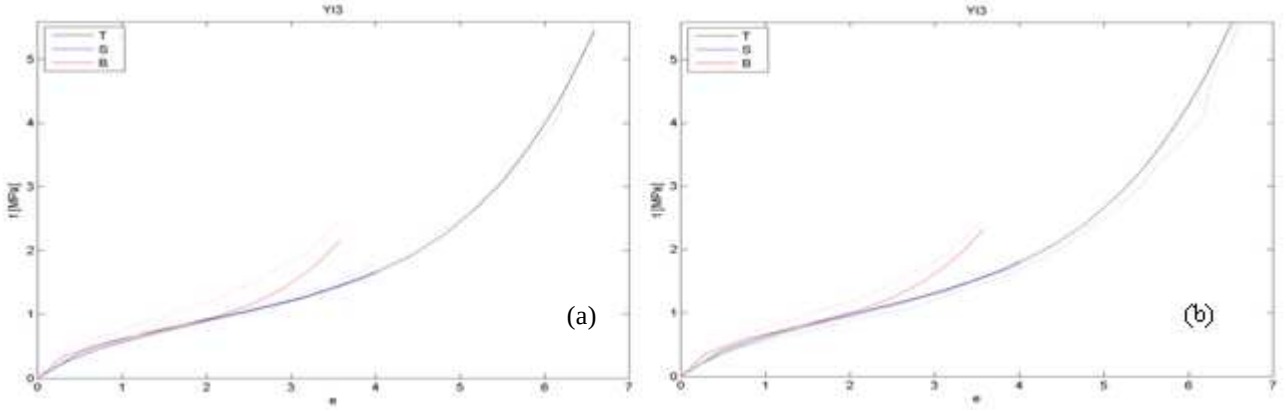

Figure 14. Predictions of the YI3 model. (a) Calibration for uniaxial mode. (b) Case 1.

However, one cannot expect that any weighting combination will bring way wrong predictions to acceptable levels. Figure 15 is showing one of such examples, where the MRI9 model failed to produce reasonable predictions for any of the combination cases analyzed. Figure 16a further explains this, since the shear and biaxial predictions are very poor. In addition, the compromise optimization in this particular case destroyed the only good prediction (Fig. 16b). That is, verification is required when using improved constants through Eq. (3), since the combination may result in predictions unable to represent suitably any of the deformation modes.

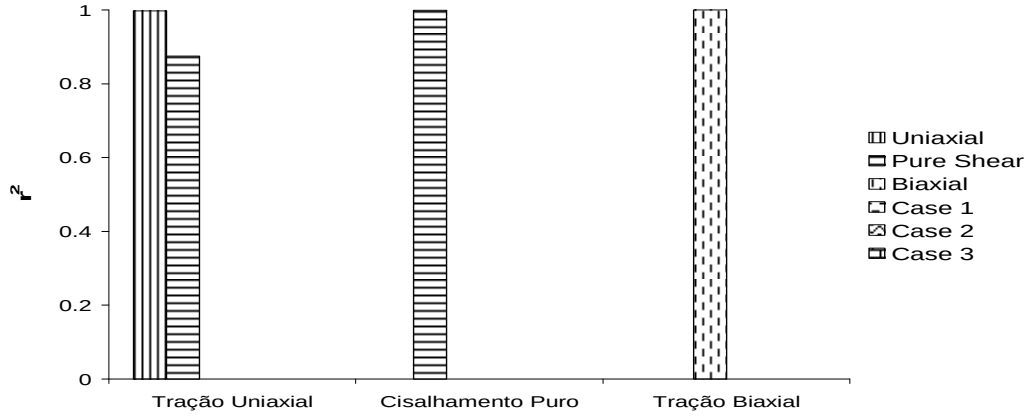

Figure 15. Compromise optimization results for MRI9 model.

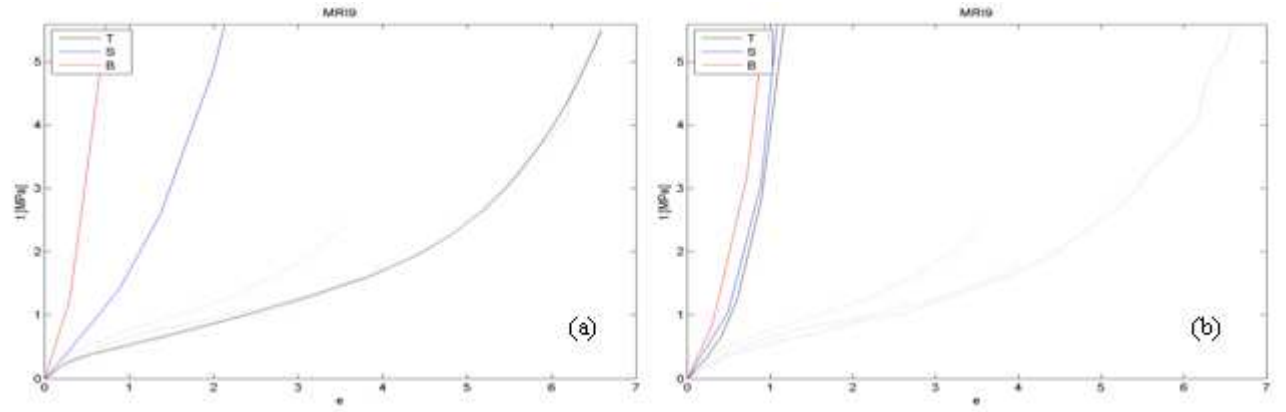

Figure 16. Predictions of the MRI9 model. (a) Calibration for for uniaxial mode. (b) Case 1.

6. CONCLUSIONS

The present work reviewed and classified many of the now popular hyperelastic models found in the literature. Their direct comparison and/or selection of a particular model by visual means is, however, a difficult task.

This work introduced a goodness of fit estimator which was successfully used to assess constitutive models as far as experimental data is available.
The proposed estimator can be directly used on $t \times e$ predictions of the material, it is a quantitative measure, removes the subjectivity of the traditional assessment methodologies, and provides a meaningful character to comparison between two or more models.

This work also investigated the performance of constitutive constants obtained by a linear combination of the ones obtained for each deformation mode. It was shown that it can be used to improve the overall performance of a given model by correcting moderately wrong predictions.

7. REFERENCES

HUMPHREY, J.D., 2002, "Cardiovascular Solid Mechanics", Springer, New York.
HUMPHREY, J.D., 2003, "Continuum biomechanics of soft biological tissues", Proc. R. Soc. Lond. A 459, pp.1-44.
HOSS, L, 2009, " Hyperelastic Constitutive Models for Incompressible Elastomers: Fitting, Performance Comparison and Proposal of a New Model", UFRGS, Porto Alegre – RS.
MARCZAK, R., HOSS, L. GHELLER, J.J., 2006, "Caracterização de Elastômeros para Simulação Numérica", Centro Tecnológico de Polímeros SENAI, São Leopoldo-RS.
TRELOAR, L., 1975, "The Physics of Rubber Elasticity", Oxford: Clarendon Press.

8. RESPONSIBILITY NOTICE

The authors Leonardo Hoss and Rogério José Marczak are the only responsible for the printed material included in this paper.